

# Mitigating Hallucination for Large Vision Language Model by Inter-Modality Correlation Calibration Decoding

Jiaming Li<sup>1\*</sup> Jiacheng Zhang<sup>2</sup> Zequn Jie<sup>3</sup> Lin Ma<sup>3</sup> Guanbin Li<sup>1,4†</sup>

<sup>1</sup>School of Computer Science and Engineering, Sun Yat-sen University, Guangzhou, China

<sup>2</sup>The University of Hong Kong <sup>3</sup> Meituan

<sup>4</sup>Research Institute, Sun Yat-sen University, Shenzhen, China

## Abstract

Large vision-language models (LVLMs) have shown remarkable capabilities in visual-language understanding for downstream multi-modal tasks. Despite their success, LVLMs still suffer from generating hallucinations in complex generation tasks, leading to inconsistencies between visual inputs and generated content. To address this issue, some approaches have introduced inference-time interventions, such as contrastive decoding and attention rectification, to reduce overreliance on language priors. However, these approaches overlook hallucinations stemming from spurious inter-modality correlations. In this paper, we propose an Inter-Modality Correlation Calibration Decoding (IMCCD) method to mitigate hallucinations in LVLMs in a training-free manner. In this method, we design a Cross-Modal Value-Enhanced Decoding (CMVED) module to alleviate hallucination by a novel contrastive decoding mechanism. During the estimation of distorted distribution, CMVED masks the value vectors associated with significant cross-modal attention weights, which address both uni-modality overreliance and misleading inter-modality correlations. Additionally, a Content-Driven Attention Refinement (CDAR) module refines cross-modal attention weights, guiding LVLMs to focus on important visual content. Experimental results on diverse hallucination benchmarks validate the superiority of our method over existing state-of-the-art techniques in reducing hallucinations in LVLM text generation. Our code will be available at <https://github.com/lijm48/IMCCD>.

## 1. Introduction

With advances in computational power and data availability, large language models [1, 2, 9, 30, 31] (LLMs) have

\*Work done during an internship at Meituan.

†The corresponding author is Guanbin Li. This research was supported by Meituan.

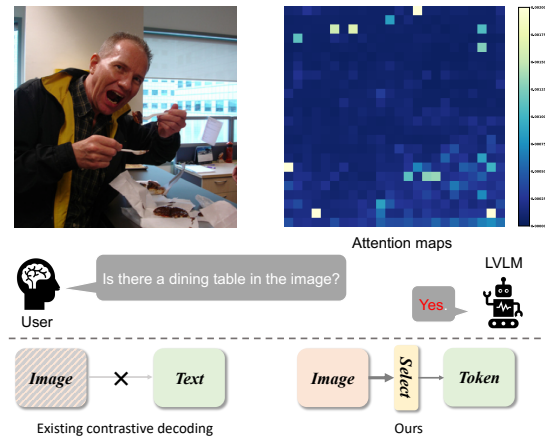


Figure 1. An example to illustrate the spurious inter-modality correlation. The figure shows significant inter-modality attention between the text about the dining table and the food in the visual content, which leads to the hallucination of the object’s existence. Existing decoding methods overlook the inter-modality correlation by distorting the image content, while our method preserves the inter-modality correlations by a selective mechanism.

achieved significant progress in language understanding, generation, and reasoning. Large vision-language models [3–6, 24, 25] (LVLMs) further extend large language models (LLMs) to vision-language tasks, demonstrating impressive performance across a range of applications, including image captioning and visual question answering. Despite these advancements, LVLMs suffer from the issue of hallucinations while generating the response, in which LVLMs generate textual content that is semantically coherent but inconsistent with ground-truth objects in the given image, hindering their reliable application.

Numerous research efforts have been dedicated to tackling the hallucination of LVLMs. Recently, contrastive decoding [21, 27] has emerged and become one of the mainstream hallucination mitigation methods. It reduces the occurrence of the hallucination by penalizing the hallucinated outputs via distribution contrasting. Specifically, con-

trastive decoding refines the output distribution of the next token by contrasting it against a distorted distribution designed to exacerbate hallucinations. The primary challenge in contrastive decoding lies in designing an effective distortion that accentuates hallucinations. To achieve this, some recent studies [11, 18, 34] propose to distort the visual content to exacerbate the overreliance on language prior. However, these methods primarily focus on the unimodal correlation, ignoring the hallucination caused by the spurious inter-modality correlations [17], which exhibit statistically significant cross-modal associations while not implying causal connections. As shown in Figure. 1, the overreliance on the spurious inter-modality correlations (food in image and dining table in query text) leads to hallucination within the generated response. Since the visual content in the current decoding methods is distorted, the inter-modality correlations are also eliminated during the distortion, leading to the overlook of spurious inter-modality correlations. Besides, ICD [32] proposes to disturb input instruction by adding a role prefix for LVLMs. However, the disturbance on language content leads to suboptimal distribution estimation from spurious inter-modality correlations.

To this end, we introduce **Inter-Modality Correlation Calibration Decoding (IMCCD)** framework for more effective hallucination mitigation. Specifically, a *Cross-Modal Value-Enhanced Decoding (CMVED)* module is devised to enhance the significant inter-modality correlation by contrastive decoding. CMVED performs distortion by selectively masking the value vectors associated with high cross-modal attention weights in self-attention layers, which suppresses important inter-modality correlations while retaining the spurious ones in distorted distribution. Unlike previous methods, CMVED’s selective distortion does not interfere with uni-modal information exchange during distribution estimation, which preserves the impact of uni-modality overreliance. By contrasting the distorted distribution that favors hallucination, CMVED facilitates the mitigation of uni-modality overreliance and spurious inter-modality correlations simultaneously. In addition, a *Content-Driven Attention Refinement (CDAR)* module is developed to mitigate the tendency to overlook essential visual tokens and alleviate the spurious inter-modality correlations led by position embeddings. This is achieved by refining the attention weights with content-driven attention weights, which are computed by normalizing the position indices of all image tokens to a uniform value.

Extensive experiments on various hallucination benchmarks of VLMs demonstrate the superiority of our IMCCD framework, exceeding the existing method by clear margins. Our contributions are summarized as follows:

- We propose a novel inter-modality correlation calibration decoding framework (IMCCD) for LVLm hallucination mitigation, which succeeds in eliminating both uni-

modality overreliance and spurious inter-modality correlations by contrastive decoding.

- We design a content-driven attention refinement module, which alleviates the overlook of visual content by refining the attention weights with content-driven attention logits.
- Comprehensive experiments on various benchmarks demonstrate the effectiveness and generalizability of our proposed method in reducing hallucinations for LVLMs.

## 2. Related works

**Large Vision-Language models.** Large vision-language models (LVLMs) equip large language models (LLMs) with the capability to perceive and understand both textual input and visual input data. The most common practice to achieve LVLMs is to integrate pre-trained LLMs with additional visual encoders and cross-modal interfaces for cross-modal fusion. For example, the LVLMs [3–6] represented by InternVL [6] introduce linear projections to map the image features from the vision encoder to the token space of LLMs. While LLaVA series [24, 25] develop a vision-language model by connecting a vision encoder and an LLM with a projection layer and fine-tuning their model based on their generated instructional vision-language data. Instead, another line of work [19, 36, 37, 45] such as BLIP-2 [19] adopts the design of query transformer as the interface between vision encoders and LLMs. Dai et al. [10] further proposes InstructBLIP, which enhances visual comprehension through vision-language instruction tuning and introduces instruction-aware visual feature extraction to query transformers to enable context-relevant processing of visual content based on the given instructions. Despite these advancements in LVLMs, these models continue to struggle with severe hallucination issues, where generated content misaligns with the visual inputs. Our work aims to mitigate the hallucination of current LVLMs and facilitates the application of LVLMs in various domains.

**Hallucination in LVLMs.** The hallucination problem was first discovered in the field of LLMs. It refers to the misalignment between the generated content from LLMs and real-world facts (namely the factuality hallucination) or user instruction (namely the faithfulness hallucination). Built upon LLMs, LVLMs also suffer from the hallucination that manifests as a misalignment between generated text and the visual input. Various approaches have been proposed to tackle this issue, including the works from the perspective of constructing additional robust training instruction [15, 23, 39, 42], reinforcement learning with human/AI feedback [12, 16, 20, 29, 40, 41], or model structure enhancement [43], etc. Despite achieving impressive results, these methods always require extensive data collection or additional fine-tuning of LVLMs, making them both computationally and labor-intensive. An-

other line of method [13, 26, 33, 35, 38, 44] focuses on the training-free method by improving the inference process of LVLMs to suppress hallucination. For example, some methods [7, 11, 14, 18, 32, 34] mitigate the hallucination via reducing the over-reliance of LVLMs on the language prior by performing conservative decoding on the original inputs and the inputs with disturbed contents. Similarly, other methods like VCD [18] propose to distort the visual content by noise-adding [18] or token-wise pruning [11, 34], while ICD [32] distorts the instruction by introducing the negative role prefix for LVLMs. However, the distortion of textual/visual content intervenes in cross-modal attention, neglecting hallucinations caused by spurious inter-modality correlations, which is the focus of this work.

### 3. Methodology

#### 3.1. Preliminaries

Modern LVLMs generally consist of a visual encoder, a cross-modal interface, and a language decoder. The visual encoder is typically adapted from a pre-trained vision model, while the language decoder is derived from a pre-trained LLM. During inference, LVLMs process both visual and textual inputs to iteratively generate the next token in the response sequence. Specifically, the visual encoder first encodes the input visual content into visual features. The cross-modal interface then maps these visual features to the input space of the language decoder to generate the image tokens  $\mathbf{X} = \{x_i\}_{i=0}^n$ . Here  $x_i$  is the image token corresponding to the  $i$ -th patch of the image and  $n$  is the number of patches. Besides, the text input is mapped to the text tokens  $\mathbf{T} = \{t_i\}_{i=0}^m$ , where  $t_i$  is  $i$ -th text token and  $m$  is the number of text tokens. The image tokens and text tokens are then concentrated to generate the input tokens  $[\mathbf{T}_{0:m_b}, \mathbf{X}, \mathbf{T}_{m_b+1:m}]$  for the language decoder.  $\mathbf{T}_{0:m_b} = \{t_i\}_{i=0}^{m_b}$  is the first  $m_b$  tokens (system prompt) in  $\mathbf{T}$  and  $\mathbf{T}_{m_b+1:m} = \{t_i\}_{i=m_b+1}^m$  is the remaining part of  $\mathbf{T}$ . **Language Decoder Forwarding.** The multi-head self-attention layer is commonly used in the language decoder. During the forward of the language decoder, the input tokens are initially transformed into input embeddings by the embedding layer, which then serves as hidden states for the first self-attention layer. For each input sample, every head within a self-attention layer maps the hidden states to queries  $\mathbf{Q} \in \mathbb{R}^{(n+m) \times d}$ , keys  $\mathbf{K} \in \mathbb{R}^{(n+m) \times d}$ , and values  $\mathbf{V} \in \mathbb{R}^{(n+m) \times d}$  by linear transformation. Here  $(n+m)$  is the sequent length of input tokens and  $d$  denotes the hidden dimensions. Then, the attention matrix  $\mathbf{A} \in \mathbb{R}^{(n+m) \times (n+m)}$  is estimated based on  $\mathbf{Q}$  and  $\mathbf{K}$  by,

$$\mathbf{A}^l = \frac{\mathbf{Q}\mathbf{K}^T}{\sqrt{d}}, \mathbf{A} = \text{softmax}(\mathbf{A}^l), \quad (1)$$

where  $\mathbf{A}^l$  is the attention logits before softmax. The atten-

tion matrix  $\mathbf{A}$  estimates the relevance of each token, which is used to reweight the values  $\mathbf{V}$  from each token to obtain the attention output  $\mathbf{O} \in \mathbb{R}^{(n+m) \times d}$ ,

$$\mathbf{O} = \mathbf{A}\mathbf{V}, \quad (2)$$

The attention output  $\mathbf{O}$  is subsequently fed into the fully connected feed-forward network (FFN), whose output then serves as the input hidden states for the subsequent multi-head self-attention layer.

**Next Token Prediction.** The language decoder parameterized by  $\theta$  in LVLMs generates the  $t$ -th output token based on the text tokens  $\mathbf{T}$ , image tokens  $\mathbf{X}$ , and the previously generated tokens  $\mathbf{Y}_{<t}$  in an auto-regressive manner. This process can be formulated as follows,

$$\begin{aligned} \mathbf{Y}_t &\sim p_\theta(\mathbf{Y}_t | \mathbf{T}, \text{Attn}(\mathbf{O} | \mathbf{T}, \mathbf{X}, \mathbf{Y}_{<t})), \\ &\propto \text{logit}_\theta(\mathbf{Y}_t | \text{Attn}(\mathbf{O} | \mathbf{T}, \mathbf{X}, \mathbf{Y}_{<t})), \end{aligned} \quad (3)$$

where  $p_\theta(\cdot)$  and  $\text{logit}_\theta(\cdot)$  denote the output probability scores and logits of language decoder, respectively.  $\text{Attn}$  is the self-attention process by Eq.1 and 2. The output token  $\mathbf{Y}_t$  is subsequently concentrated with previously generated tokens to serve as input for the next step in the token generation sequence.

**Contrastive Decoding for LVLMs.** Contrastive Decoding [18] is an effective training-free intervention strategy to suppress hallucination. The core idea is to take the extra manually crafted distorted textual or visual content as input and then contrast the output distribution derived from the original input against the distorted counterpart, which alleviates the overreliance on individual modal priors and subsequently reduces the occurrence of the hallucination. Formally, contrastive decoding can be formulated as:

$$\mathbf{l}_t = \text{logit}_\theta(\mathbf{Y}_t | \text{Attn}(\mathbf{O} | \mathbf{T}, \mathbf{X}, \mathbf{Y}_{<t})) \quad (4)$$

$$\tilde{\mathbf{l}}_t = \text{logit}_\theta(\mathbf{Y}_t | \text{Attn}(\mathbf{O} | \tilde{\mathbf{T}}, \tilde{\mathbf{X}}, \mathbf{Y}_{<t})) \quad (5)$$

$$p_\theta(\mathbf{Y}_t | \mathbf{T}, \mathbf{X}) = \text{softmax}((1 + \alpha)\mathbf{l}_t - \alpha\tilde{\mathbf{l}}_t). \quad (6)$$

$\alpha$  is the hyper-parameter controlling the contrastive effect. Despite widely studied [7, 14, 18, 32, 34], existing methods primarily focus on the unimodal distortion, neglect the spurious inter-modality correlations, leading to suboptimal estimation of distorted distribution.

#### 3.2. IMCCD for LVLMs Hallucination Mitigation

In this section, we introduce the **Inter-Modality Correlation Calibration Decoding (IMCCD)** framework to mitigate the hallucination in LVLMs. IMCCD comprises two key designs, namely **Cross-modal Value-enhanced Decoding (CMVED)** and **Content-Driven Attention Refinement (CDAR)**, alleviating both the spurious inter-modality correlations and uni-modality over-reliance. The overview of our method is illustrated in Figure. 2.

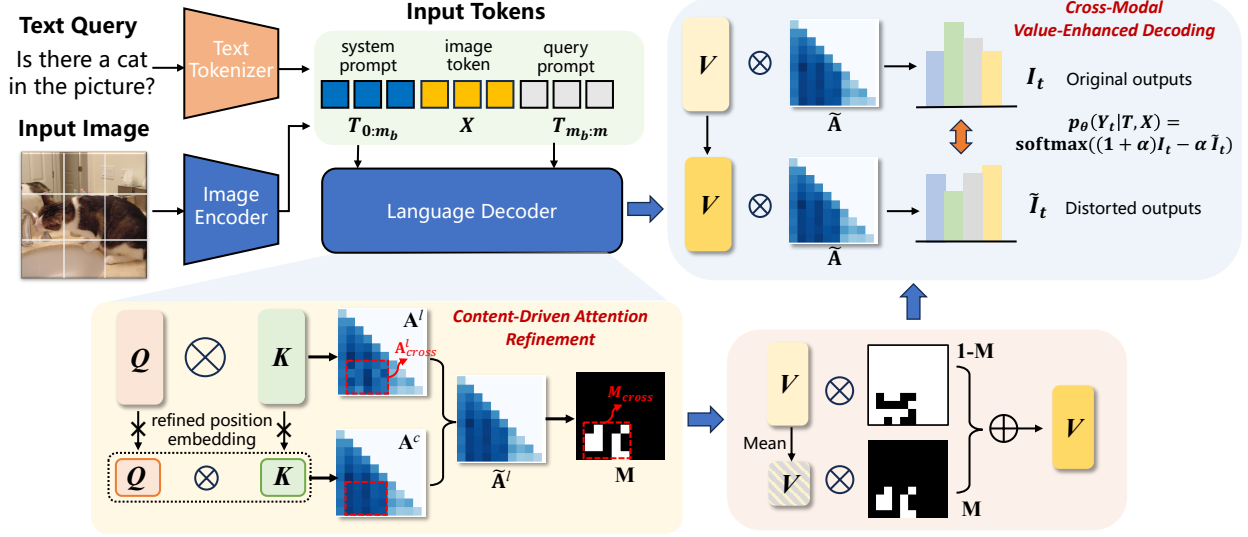


Figure 2. An overview of the proposed IMCCD approach, consisting of two modules: Cross-modal Value-enhanced Decoding (CMVED) and Content-Driven Attention Refinement (CDAR). During inference, CMVED generates a distorted output distribution that favors hallucination by selectively masking value vectors corresponding to high attention weights in the cross-modal segment of the attention matrix. CMVED then performs contrastive decoding between the original outputs and distorted outputs to mitigate the hallucination. Additionally, CDAR refines the cross-modal segments of attention logits with content-driven attention logits estimated by normalizing the position indices of all image tokens to a uniform value.

### 3.2.1 Cross-Modal Value-Enhanced Decoding

Existing contrastive decoding methods primarily focus on the hallucination stemming from the over-reliance on the uni-modal prior by distorting the textual or visual content, ignoring the hallucination caused by the spurious inter-modality correlation. To this end, we propose cross-modal value-enhanced decoding (CMVED), which performs inter-modality correlation correction via the distortion on the level of cross-modal attention.

Our key insight is to selectively suppress the value vectors corresponding to high values in attention logits and exacerbate the hallucination from the inter-modality interaction, thus subsequently alleviating it with contrastive decoding. Concretely, from attention logits  $\mathbf{A}^l \in \mathbb{R}^{(n+m) \times (n+m)}$ , we isolate the cross-modal segment, which is denoted as  $\mathbf{A}_{\text{cross}}^l = \mathbf{A}^l[m_b + n : m + n, m_b : m_b + n]$ .  $\mathbf{A}_{\text{cross}}^l$  specifically represents the attention weights between image tokens and subsequent text tokens, capturing the inter-modality correlations within the self-attention layer. Based on such cross-modal attention weight, we aim to estimate the distribution that favors the hallucination, which afterward is used to mitigate the hallucination from spurious inter-modality correlations. To accomplish this, CMVED first generates a mask that selectively identifies the prominent attention weights based on their magnitude,

$$\mathbf{M}_{\text{cross}} = \mathbb{I}(\mathbf{A}_{\text{cross}}^l < \mu(\mathbf{A}_{\text{cross}}^l)), \quad (7)$$

where  $\mu(\cdot)$  represents the mean operation and  $\mathbb{I}$  is the indicator function. The binary mask  $\mathbf{M}_{\text{cross}} \in \mathbb{R}^{(m-m_b) \times (n)}$  adaptively indicates the selected significant attention weights for the cross-modal segment. We subsequently pad the  $\mathbf{M}_{\text{cross}}$  to a global mask  $\mathbf{M} \in \mathbb{R}^{(n+m) \times (n+m)}$  which applies to all attention weights in  $\mathbf{A}$  with zero padding. Specifically,  $\mathbf{M}[m_b + n : m + n, m_b : m_b + n]$  is set to the  $\mathbf{M}_{\text{cross}}$ , ensuring that the cross-modal part is accurately masked in the global context.

With this global mask, CMVED then distorts the cross-modal segment of self-attention. While recent approaches typically adapt token-wise pruning image tokens, CMVED masks the value vector  $\mathbf{V}$  to  $\mu(\mathbf{V})$  by dim-wise mean operation to exacerbate the hallucination. With this process, the content of the value vector is teased apart. CMVED then estimates the attention output by performing the weighted sum between the origin value vector  $\mathbf{V}$  and distorted value vector  $\mu(\mathbf{V})$  guided by both the mask  $\mathbf{M}$  and attention weights  $\mathbf{A}$ . Specifically, CMVED modifies the process Eq. 2 by the following process,

$$\tilde{\mathbf{O}} = (\mathbf{M} \cdot \mathbf{A})\mu(\mathbf{V}) + ((1 - \mathbf{M}) \cdot \mathbf{A})\mathbf{V}. \quad (8)$$

With the above equation, CMVED distorts the value vectors corresponding to the significant cross-modal attention weights while keeping the value vectors of the remaining attention part unchanged, which suppresses important inter-modality correlations from cross-modal attention. Similar

to Eq. 6, the final contrastive decoding process is performed by the following equations,

$$\mathbf{l}_t = \text{logit}_\theta(\mathbf{Y}_t | \text{Attn}(\mathbf{O} | \mathbf{T}, \mathbf{X}, \mathbf{Y}_{<t})) \quad (9)$$

$$\tilde{\mathbf{l}}_t = \text{logit}_\theta(\mathbf{Y}_t | \text{Attn}(\tilde{\mathbf{O}} | \mathbf{T}, \mathbf{X}, \mathbf{Y}_{<t})) \quad (10)$$

$$p_\theta(\mathbf{Y}_t | \mathbf{T}, \mathbf{X}) = \text{softmax}((1 + \alpha)\mathbf{l}_t - \alpha\tilde{\mathbf{l}}_t). \quad (11)$$

Compared with recent contrastive decoding methods, the advantages of CMVED are three folds: (1) The distortion process used in CMVED directly focuses on the cross-modal segment of attention to alleviate the cross-modal inconsistency. Specifically, it proposes to modify the value vectors with high attention weights on cross-modal attention, leaving the low-weight inter-modality correlations and intra-modality knowledge exchange unaffected. This approach enables CMVED to address hallucinations from both uni-modality overreliance and spurious inter-modality correlations more effectively. (2) Traditional contrastive decoding methods alter attention weights from visual tokens to text tokens, which can result in over- or under-estimated hallucinations from image regions. CMVED, however, avoids modifying attention weights, yielding a more precise estimation of distributions prone to hallucination. (3) Besides, since the attention process of the visual part remains the same, the key and value vectors and attention weights can be directly derived from the original forward process, leading to a faster inference time than other contrastive decoding methods.

### 3.2.2 Content-Driven Attention Refinement

Although CMVED reduces hallucinations arising from the cross-modal interaction, MLLMs still face challenges with visual content retention. Specifically, with the position embeddings, the text tokens will be biased to pay more attention to the latter part of the image visual tokens, while overlooking the initial visual tokens, leading to more hallucinations. Figure. 3 illustrates the distribution of attention weights from the text tokens to the image tokens. It can be observed that attention is often directed toward the latter visual tokens rather than the relevant ones. Despite the last few visual tokens that may act as summary tokens to summarize the image content, this pattern amplifies the forgetting of initial visual tokens, which are more distanced from text tokens. Consequently, the positional relations among different image tokens with text tokens are less critical than other positional relations, including the positional relations among different text tokens and the global position of image in the text input.

Motivated by this, we propose content-driven attention refinement (CDAR) to encourage the self-attention layer to prioritize the actual relevant content of visual tokens over their positional ordering within images. Concretely, in the



Figure 3. An example to illustrate the over-reliance on the latter part of image tokens. The text tokens of LLM pay more attention to the nearest image tokens than that of other image tokens, leading to the hallucination about the existence of TV.

first  $l$  attention layer of the language decoder, we estimate new position indexes by normalizing the position indices of all image tokens to a uniform value. It is achieved by replacing the original position indexes of concentrated input tokens, noted with  $\mathbf{P} = [\{i\}_{i=1}^{m+n}]$ , with refined position indexes,

$$\mathbf{P}^c = [\{i\}_{i=1}^{m_b}, \{m_b + 1\}_{i=1}^n, \{i + 1\}_{i=m_b+1}^m]. \quad (12)$$

The refined position indexes keep the global positional relation of the image content in the input language while teasing apart the positional relations among different image tokens with other language tokens. The modified position indexes  $\mathbf{P}^c$  is used to perform ROPE to queries  $\mathbf{Q}$  and keys  $\mathbf{K}$  to estimate the attention logits  $\mathbf{A}^c$  with refined position embeddings by Eq. 1. Then we refine the cross-modal part of attention logits  $\mathbf{A}^l$  with,

$$\tilde{\mathbf{A}}_{i,j}^l = \begin{cases} \gamma \mathbf{A}_{i,j}^c + (1 - \gamma) \mathbf{A}_{i,j}^l, & \text{if } j > m^b + n \\ & \text{and } m^b + n > i \geq m^b, \\ \mathbf{A}_{i,j}^l, & \text{otherwise.} \end{cases}$$

$\gamma$  is the hyperparameter controlling the proportion of  $\mathbf{A}^c$ . Note that this refinement is applied to both the estimation of logits from original inputs and distorted inputs. Specifically, the  $\mathbf{A}_{\text{cross}}^l$  in Eq. 7 and  $\mathbf{A}$  in Eq. 2, Eq. 8 are replaced with  $\tilde{\mathbf{A}}_{\text{cross}}^l$  and  $\tilde{\mathbf{A}}$ , respectively.  $\tilde{\mathbf{A}}_{\text{cross}}^l$  is the cross-modal segment of  $\tilde{\mathbf{A}}^l$  and  $\tilde{\mathbf{A}} = \text{softmax}(\tilde{\mathbf{A}}^l)$  is the refined attention weights. With CDAR, the language decoder is encouraged to prioritize image content over token positions, effectively mitigating hallucinations caused by the overlook of visual content.

## 4. Experiments

### 4.1. Datasets and Evaluation Metrics

We evaluate our method on the widely used benchmarks of LVLMs hallucination mitigation, including POPE and MME following the practice of VCD [18]. In addition, we instantiate our method with the image captioning task and report the results via CHAIR metrics on the MS-COCO validation set.

**POPE.** POPE [22] designs a new metric and benchmark to assess object hallucination in the VQA paradigm. It achieves the evaluation of object hallucination in a binary classification task by prompting LVLMs to answer yes or no for short questions about the existence of probing objects (*e.g.*, Is there a car in the image?). The POPE benchmark consists of nine different subsets from three datasets, MS-COCO, AOKVQA, and GQA with three different negative sampling strategies (Random, Popular, and Adversarial). Each sampled subset includes 500 images with 6 problems for each image. Following previous works [17, 32], we add a "Please answer in one word." constraint for evaluating the POPE dataset at the end of the query text. F1-score and Accuracy are commonly reported as the metrics for the performance of hallucination mitigation on this benchmark.

**Chair.** The CHAIR [28] is a widely used metric for assessing the hallucination in responses of LVLMs. The CHAIR metric comprises two variants, namely the CHAIR<sub>i</sub> and CHAIR<sub>s</sub>, which are formulated as follows:

$$\text{CHAIR}_i = \frac{|\{\text{hallucinated objects}\}|}{|\{\text{all objects mentioned}\}|},$$
$$\text{CHAIR}_s = \frac{|\{\text{sentences with hallucinated object}\}|}{|\{\text{all sentences}\}|}.$$

Besides, we also report the recall and F1-score to show the completeness of the generated caption of the image. Following previous work [13], we randomly sample 500 images in the validation set of MS-COCO and conduct the evaluation of CHAIR metrics on the sampled subset for the image captioning task with the prompt "Please describe this image in detail".

**MME.** The MME dataset is a comprehensive benchmark for the evaluation of LVLMs. Similar to POPE, these tasks are formulated as binary classifications with yes-no questions. It encompasses 14 subtasks for the examination of the perception and cognition abilities of LVLMs. The score is estimated by the sum of the accuracy of each question and the accuracy of each image. For hallucination evaluation, we report the results on both the MME full set and the hallucination subset with four hallucination-related sub-tasks, including object existence, count, position, and color.

### 4.2. Models and Implementation Details

We integrate our proposed method with two popular LVLMs, LLaVA1.5 [24] and InstructBLIP [10]. Both the two models adopt Vicuna 7B [8] as their language models. We empirically set  $l = 3$  and  $\gamma = 0.2$ . We set the  $\alpha = 3$  for the POPE dataset and  $\alpha = 1$  for others, leaving other hyper-parameters the same with VCD.

### 4.3. Experimental Results

**Comparison on POPE.** We compare our method against three existing contrastive decoding methods, including VCD [18] and ICD [32], on the POPE dataset. The results are presented in Table 1. It can be observed that our method boosts the performance of LVLMs in mitigating hallucination from object existence for each setup of different subsets on POPE. Our proposed IMCCD method outperforms the existing methods ICD and VCD by a clear margin both on LLaVA 1.5 and InstructBLIP. Compared to VCD, IMCCD achieves a notable increase in accuracy (ranging from 0.76% to 3.27%) and F1 score (ranging from 0.53% to 2.57%), underscoring its effectiveness in reducing spurious inter-modality correlations. Additionally, IMCCD improves precision and recall in most setups, showcasing its robustness in generating both accurate and comprehensive responses.

**Comparison on CHAIR.** We conduct evaluation of the CHAIR metric on the MS-COCO validation set in Table 2 to validate the performance of our method on the image captioning task and long sequence generation. It shows that the performance of our method is better than that of other existing contrastive decoding methods. Specifically, our IMCCD significantly enhances the performance of LVLMs on CHAIR<sub>i</sub> and CHAIR<sub>s</sub> by 5.8% and 4.0% for LLaVA 1.5 and by 5.7% and 3.2% for InstructBLIP, demonstrating the capability of our method for generating long sequence response with less hallucination. Besides, our IMCCD also achieves a better recall and F1 score, which showcases that the generated responses from our method can describe the image content more accurately and more completely.

**Comparison on MME.** To validate the effectiveness of our method in mitigating various types of hallucination beyond object existence, we perform the comparison on the MME hallucination subset and the MME full set. For MME hallucination set shown in Table 3, IMCCD achieves the best scores on mitigating both object-level and attribute-level hallucination. Beyond the object existence, IMCCD leads to an improvement of 15.00, 5.59, and 4.17 on count, position, and color for LLaVA1.5, which demonstrates the generalization capability of our method across various types of hallucinations.

For the MME full set, Figure 4 illustrates the performance of LLaVA 1.5 with normal decoding, VCD, and our method. Our method generally outperforms the other meth-

Dataset	Setup	Method	LLaVA 1.5				InstructBLIP			
			Accuracy	Precision	Recall	F1 Score	Accuracy	Precision	Recall	F1 Score
MS-COCO	Random	Baseline	83.29	92.13	72.80	81.33	80.71	81.67	79.19	80.41
		VCD	87.73	91.42	83.28	87.16	84.53	88.55	79.32	83.68
		ICD	85.17	<b>95.99</b>	73.40	83.19	<u>86.43</u>	92.01	<b>80.73</b>	<u>85.61</u>
		Ours	<b>89.23</b>	93.50	<b>84.33</b>	<b>88.68</b>	<b>86.96</b>	<b>93.97</b>	79.00	<b>85.83</b>
	Popular	Baseline	81.88	88.93	72.80	80.06	78.22	77.87	78.85	78.36
		VCD	85.38	86.92	<b>83.28</b>	85.06	81.47	82.89	79.32	81.07
		ICD	82.33	82.25	<u>82.47</u>	82.36	82.93	84.45	<b>80.73</b>	<u>82.55</u>
		Ours	<b>86.73</b>	<b>90.22</b>	<u>82.40</u>	<b>86.13</b>	<b>84.20</b>	<b>89.34</b>	77.67	<b>83.10</b>
	Adversarial	Baseline	78.96	83.06	72.75	77.57	75.84	74.30	79.03	76.59
		VCD	80.88	79.45	<b>83.29</b>	81.33	79.56	79.67	79.39	79.52
		ICD	81.17	<b>87.13</b>	73.13	79.52	80.87	80.95	<b>80.73</b>	80.84
		Ours	<b>82.87</b>	83.22	<u>82.33</u>	<b>82.77</b>	<b>82.57</b>	<b>86.10</b>	77.67	<b>81.67</b>
A-OKVQA	Random	Baseline	83.45	87.24	78.36	82.56	80.91	77.97	86.16	81.86
		VCD	86.15	85.18	<u>87.53</u>	86.34	84.11	82.21	87.05	84.56
		ICD	86.20	<b>91.07</b>	<u>80.27</u>	85.33	<u>85.82</u>	83.80	<b>88.94</b>	<u>86.29</u>
		Ours	<b>88.27</b>	88.11	<b>88.47</b>	<b>88.29</b>	<b>87.03</b>	<b>88.71</b>	84.87	<b>86.75</b>
	Popular	Baseline	79.90	80.85	78.36	79.59	76.19	72.16	85.28	78.17
		VCD	81.85	78.60	<b>87.53</b>	82.82	79.78	76.00	87.05	81.15
		ICD	82.63	<b>84.25</b>	80.27	82.21	<u>81.64</u>	78.50	<b>88.77</b>	<b>83.32</b>
		Ours	<b>85.13</b>	<u>84.13</u>	<u>86.60</u>	<b>85.35</b>	<b>82.23</b>	<b>79.86</b>	86.20	<u>82.91</u>
	Adversarial	Baseline	74.04	72.08	78.49	75.15	70.71	65.91	85.83	75.56
		VCD	74.97	70.01	<u>87.36</u>	77.73	<u>74.33</u>	<u>69.46</u>	86.87	77.19
		ICD	77.20	<b>75.47</b>	80.60	77.95	<u>74.42</u>	<u>70.24</u>	<b>88.93</b>	<b>78.48</b>
		Ours	<b>77.90</b>	73.85	<b>86.40</b>	<b>79.63</b>	<b>75.37</b>	<b>71.03</b>	85.67	<u>77.67</u>
GQA	Random	Baseline	83.73	87.16	79.12	82.95	79.75	77.14	84.29	80.56
		VCD	86.65	84.85	<u>89.24</u>	86.99	83.69	81.84	<b>86.61</b>	84.16
		ICD	85.73	<b>90.79</b>	79.53	84.79	85.10	84.21	86.40	85.29
		Ours	<b>89.53</b>	<u>90.62</u>	<b>88.20</b>	<b>88.80</b>	<b>86.03</b>	<b>87.67</b>	83.87	<b>85.72</b>
	Popular	Baseline	78.17	77.64	79.12	78.37	73.87	69.63	84.69	76.42
		VCD	80.73	76.26	<b>89.24</b>	82.24	78.57	74.62	86.61	80.17
		ICD	79.87	80.07	79.53	79.80	<u>78.80</u>	<u>75.15</u>	<b>87.53</b>	<b>80.87</b>
		Ours	<b>84.73</b>	<b>82.48</b>	88.20	<b>85.24</b>	<b>79.57</b>	<b>76.23</b>	85.93	<u>80.79</u>
	Adversarial	Baseline	75.08	73.19	79.16	76.06	70.56	66.12	84.33	74.12
		VCD	76.09	70.83	<b>88.75</b>	78.78	75.08	<u>70.59</u>	85.99	77.53
		ICD	77.60	<u>76.04</u>	80.60	78.25	75.17	<u>70.59</u>	<b>86.27</b>	77.65
		Ours	<b>80.17</b>	<b>76.11</b>	<u>87.93</u>	<b>81.60</b>	<b>77.03</b>	<b>73.37</b>	84.87	<b>78.70</b>

Table 1. **Results on discrimination hallucination benchmark POPE.** The Baseline method denotes the standard decoding. The best performances within each setting are **bolded**. Comparable ( $\pm 1.0$ ) but not the best performances are underlined. We implemented ICD for LLaVA 1.5 in our evaluation setup.

Method	LLaVA 1.5				InstructBLIP			
	CHAIR <sub>i</sub> ↓	CHAIR <sub>s</sub> ↓	Recall ↑	F1 Score ↑	CHAIR <sub>i</sub> ↓	CHAIR <sub>s</sub> ↓	Recall ↑	F1 Score ↑
Baseline	55.6	17.8	72.4	77.0	57.0	16.7	70.4	76.3
VCD	54.2	16.4	76.7	80.0	53.6	15.6	<b>74.6</b>	79.2
ICD	54.0	15.4	<b>77.2</b>	80.7	49.6	14.5	72.6	78.5
Ours	<b>49.8</b>	<b>13.8</b>	76.7	<b>81.2</b>	<b>51.3</b>	<b>13.5</b>	73.6	<b>79.9</b>

Table 2. **Results on hallucination metric CHAIR on the MS-COCO validation set.** The Baseline method denotes the standard decoding. The best performances within each setting are **bolded**.

ods in 10 sub-tasks of 14. Notably, our method demonstrates a strong capability for perception, outperforming VCD and ICD by a large margin. However, our approach is less effective in numerical calculations and text translation tasks, as these primarily rely on the language de-

coder’s reasoning capability rather than visual content comprehension. Nevertheless, our method maintains comparable performance in recognition tasks compared to existing approaches. Overall, these findings illustrate that our method enhances the general functionality of LVLMs while

Model	Decoding	Object-level		Attribute-level		Total $\uparrow$
		Existence $\uparrow$	Count $\uparrow$	Position $\uparrow$	Color $\uparrow$	
LLaVA1.5	Baseline	183.75	110.00	115.83	157.08	566.67
	VCD	186.25	116.67	119.17	159.17	581.25
	ICD	185.00	117.91	117.50	<b>162.08</b>	582.50
	Ours	<b>186.25</b>	<b>125.00</b>	<b>120.42</b>	161.25	<b>592.92</b>
InstructBLIP	Baseline	154.17	86.67	58.33	123.75	422.91
	VCD	166.67	82.08	67.08	130.00	445.83
	ICD	166.67	80.83	67.92	128.33	443.75
	Ours	<b>171.66</b>	<b>85.41</b>	<b>69.58</b>	<b>132.50</b>	<b>459.17</b>

Table 3. Results on the hallucination subset of MME. The best performances within each setting are **bolded**.

also effectively mitigating hallucinations.

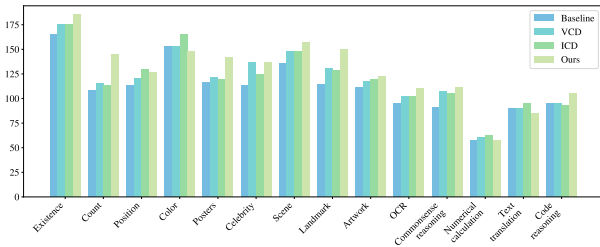


Figure 4. Results of LLaVA1.5 on MME-Fullset.

#### 4.4. Ablation Study and Analysis

In this section, we conduct ablation to demonstrate the effectiveness of our method. Without specification, our ablation study is done on the popular setups of the MS-COCO subset for POPE and the MS-COCO validation set for CHAIR.

**Impact of individual proposed modules.** We conducted an ablation study to assess the effectiveness of each individual module, including CMVED and CDAR, within our IMCCD framework. As illustrated in Table 4, CMVED significantly improves the performance by 4.98% on Accuracy and 5.45% on F1 for visual question answering task, underscoring the significance of CMVED on mitigating hallucination. The combination of CMVED and CDAR demonstrates a 0.62% performance improvement of F1, which validates the effectiveness of CDAR in alleviating the forgetting of visual content. For image-captioning tasks, CMVED boosts the performance on both CHAIR<sub>s</sub>. Based on CMVED, CDAR slightly enhances the performance, showcasing the efficacy of CDAR for long sequence generation tasks.

**Ablation of distortion used in our method.** In Table 4, We show the performance of our method with different kinds of distortions. Specifically, 'Attention mask' indicates pruning the significant attention weights by conventional attention mask strategy. 'Value noise addition' indicates adding noise

CMVED	CDAR	POPE		CHAIR	
		Accuracy	F1 Score	CHAIR <sub>i</sub>	CHAIR <sub>s</sub>
		81.88	80.06	55.6	17.8
✓		85.86	85.51	50.6	14.3
	✓	83.27	82.04	54.5	16.1
✓	✓	86.73	86.13	49.8	13.8

Table 4. Ablation of the core components on POPE COCO Popular and CHAIR COCO for LLaVA 1.5.

on value vectors similar to VCD[18] instead of masking the value vectors to the mean value, which is denoted as 'Value mask'. Our method shows a better hallucination mitigation capability compared with attention masking, which demonstrates altering the attention weights may lead to over or under-estimation of hallucinations from image regions. Besides, Value noise addition slightly improves performance on POPE but leads to a decline on CHAIR. In contrast, the value mask distortion in our method achieves a better trade-off between different kinds of tasks.

Distortion	POPE		CHAIR	
	Accuracy	F1 Score	CHAIR <sub>i</sub>	CHAIR <sub>s</sub>
Attention mask	84.27	85.63	50.7	14.5
Value noise addition	86.90	86.74	52.2	14.8
Value mask	86.73	86.13	49.8	13.8

Table 5. Ablation of different kinds of distortion used in our method.

**Analysis of hallucination with statistically significant object existence.** To assess the effectiveness of our method in mitigating hallucinations caused by spurious inter-modality correlations, we evaluate the hallucination rates of LLaVA 1.5 on the POPE dataset in scenarios with statistically significant object existence, which often induce spurious correlations. Specifically, the hallucination rate is calculated on the MS-COCO and A-OKVQA subsets, and only the objects with a high co-existence rate (over 70%) with their top co-occurring object are taken into account. Figure 5(a) illustrates that the statistically significant co-existence leads to a serious hallucination both on true negative rate and false negative rate. This finding indicates that spurious inter-modality correlations can cause both the neglect of relevant regions of interest and an over-reliance on irrelevant regions. Figure 5(b) demonstrates that our method effectively reduces both true negative and false negative hallucinations stemming from co-existence, underscoring its ability to mitigate hallucinations arising from spurious inter-modality correlations.

## 5. Conclusion

In this paper, we have introduced IMCCD, a novel framework addressing the hallucination problem of LLMs



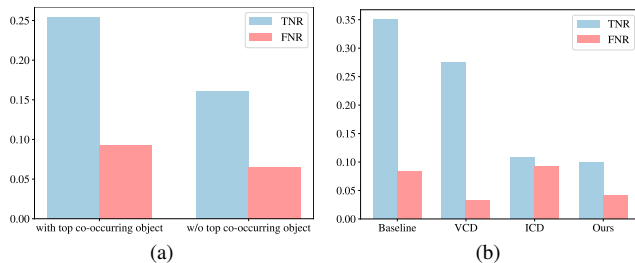


Figure 5. The comparison of the hallucination rate of LLaVA 1.5 on the POPE dataset. 'TNR' and 'FNR' denote the true negative rate and the false negative rate of VQA, respectively. (a) The hallucination rate of the existence of objects with and without the co-existence with their top co-occurring object in the image. (b) The hallucination rate of the object's existence for different decoding methods with their top co-occurring object. Concretely, we estimate the mean hallucination rate on 5 pairs of objects with a high object existence rate.

with contrastive decoding. In this approach, we propose the cross-modal value-enhanced decoding which estimates a distorted distribution favored hallucination by selectively masking the value vectors associated with high cross-modal attention weights, alleviating both the spurious inter-modality correlation and the uni-modal over-reliance. Furthermore, a Content-Driven Attention Refinement module is introduced to alleviate the overlook of essential visual content caused by position bias. Extensive experiments conducted on diverse benchmarks and LVLMs confirm the efficacy of the proposed method.

## References

- [1] Josh Achiam, Steven Adler, Sandhini Agarwal, Lama Ahmad, Ilge Akkaya, Florencia Leoni Aleman, Diogo Almeida, Janko Altenschmidt, Sam Altman, Shyamal Anadkat, et al. Gpt-4 technical report. *arXiv preprint arXiv:2303.08774*, 2023. 1
- [2] Jinze Bai, Shuai Bai, Yunfei Chu, Zeyu Cui, Kai Dang, Xiaodong Deng, Yang Fan, Wenbin Ge, Yu Han, Fei Huang, et al. Qwen technical report. *arXiv preprint arXiv:2309.16609*, 2023. 1
- [3] Jinze Bai, Shuai Bai, Shusheng Yang, Shijie Wang, Sinan Tan, Peng Wang, Junyang Lin, Chang Zhou, and Jingren Zhou. Qwen-vl: A frontier large vision-language model with versatile abilities. *arXiv preprint arXiv:2308.12966*, 2023. 1, 2
- [4] Keqin Chen, Zhao Zhang, Weili Zeng, Richong Zhang, Feng Zhu, and Rui Zhao. Shikra: Unleashing multi-modal llm's referential dialogue magic. *arXiv preprint arXiv:2306.15195*, 2023.
- [5] Zhe Chen, Weiyun Wang, Hao Tian, Shenglong Ye, Zhangwei Gao, Erfei Cui, Wenwen Tong, Kongzhi Hu, Jiapeng Luo, Zheng Ma, et al. How far are we to gpt-4v? closing the gap to commercial multimodal models with open-source suites. *arXiv preprint arXiv:2404.16821*, 2024.
- [6] Zhe Chen, Jiannan Wu, Wenhai Wang, Weijie Su, Guo Chen, Sen Xing, Muyan Zhong, Qinglong Zhang, Xizhou Zhu, Lewei Lu, et al. Internvl: Scaling up vision foundation models and aligning for generic visual-linguistic tasks. In *Proceedings of the IEEE/CVF Conference on Computer Vision and Pattern Recognition*, pages 24185–24198, 2024. 1, 2
- [7] Zhaorun Chen, Zhuokai Zhao, Hongyin Luo, Huaxiu Yao, Bo Li, and Jiawei Zhou. Halc: Object hallucination reduction via adaptive focal-contrast decoding. *arXiv preprint arXiv:2403.00425*, 2024. 3
- [8] Wei-Lin Chiang, Zhuohan Li, Zi Lin, Ying Sheng, Zhanghao Wu, Hao Zhang, Lianmin Zheng, Siyuan Zhuang, Yonghao Zhuang, Joseph E. Gonzalez, Ion Stoica, and Eric P. Xing. Vicuna: An open-source chatbot impressing gpt-4 with 90%\* chatgpt quality, 2023. 6
- [9] Wei-Lin Chiang, Zhuohan Li, Zi Lin, Ying Sheng, Zhanghao Wu, Hao Zhang, Lianmin Zheng, Siyuan Zhuang, Yonghao Zhuang, Joseph E Gonzalez, et al. Vicuna: An open-source chatbot impressing gpt-4 with 90%\* chatgpt quality. See <https://vicuna.lmsys.org> (accessed 14 April 2023), 2(3):6, 2023. 1
- [10] Wenliang Dai, Junnan Li, Dongxu Li, Anthony Meng Huat Tiong, Junqi Zhao, Weisheng Wang, Boyang Li, Pascale Fung, and Steven Hoi. Instructblip: towards general-purpose vision-language models with instruction tuning. In *Proceedings of the 37th International Conference on Neural Information Processing Systems*, Red Hook, NY, USA, 2024. Curran Associates Inc. 2, 6
- [11] Alessandro Favero, Luca Zancato, Matthew Trager, Siddharth Choudhary, Pramuditha Perera, Alessandro Achille, Ashwin Swaminathan, and Stefano Soatto. Multi-modal hallucination control by visual information grounding. In *Proceedings of the IEEE/CVF Conference on Computer Vision and Pattern Recognition*, pages 14303–14312, 2024. 2, 3
- [12] Anisha Gunjal, Jihan Yin, and Erhan Bas. Detecting and preventing hallucinations in large vision language models. In *Proceedings of the AAAI Conference on Artificial Intelligence*, pages 18135–18143, 2024. 2
- [13] Qidong Huang, Xiaoyi Dong, Pan Zhang, Bin Wang, Conghui He, Jiaqi Wang, Dahua Lin, Weiming Zhang, and Nenghai Yu. Opera: Alleviating hallucination in multi-modal large language models via over-trust penalty and retrospection-allocation. In *Proceedings of the IEEE/CVF Conference on Computer Vision and Pattern Recognition*, pages 13418–13427, 2024. 3, 6, 12
- [14] Fushuo Huo, Wenchao Xu, Zhong Zhang, Haozhao Wang, Zhicheng Chen, and Peilin Zhao. Self-introspective decoding: Alleviating hallucinations for large vision-language models. *arXiv preprint arXiv:2408.02032*, 2024. 3
- [15] Chaoya Jiang, Haiyang Xu, Mengfan Dong, Jiaying Chen, Wei Ye, Ming Yan, Qinghao Ye, Ji Zhang, Fei Huang, and Shikun Zhang. Hallucination augmented contrastive learning for multimodal large language model. In *Proceedings of the IEEE/CVF Conference on Computer Vision and Pattern Recognition*, pages 27036–27046, 2024. 2
- [16] Minchan Kim, Minyeong Kim, Junik Bae, Suhwan Choi, Sungkyung Kim, and Buru Chang. Exploiting semantic

- reconstruction to mitigate hallucinations in vision-language models. In *European Conference on Computer Vision*, pages 236–252. Springer, 2025. 2
- [17] Sicong Leng, Yun Xing, Zesen Cheng, Yang Zhou, Hang Zhang, Xin Li, Deli Zhao, Shijian Lu, Chunyan Miao, and Lidong Bing. The curse of multi-modalities: Evaluating hallucinations of large multimodal models across language, visual, and audio. *arXiv preprint arXiv:2410.12787*, 2024. 2, 6
- [18] Sicong Leng, Hang Zhang, Guanzheng Chen, Xin Li, Shijian Lu, Chunyan Miao, and Lidong Bing. Mitigating object hallucinations in large vision-language models through visual contrastive decoding. In *Proceedings of the IEEE/CVF Conference on Computer Vision and Pattern Recognition*, pages 13872–13882, 2024. 2, 3, 6, 8, 12
- [19] Junnan Li, Dongxu Li, Silvio Savarese, and Steven Hoi. Blip-2: Bootstrapping language-image pre-training with frozen image encoders and large language models. In *International conference on machine learning*, pages 19730–19742. PMLR, 2023. 2
- [20] Lei Li, Zhihui Xie, Mukai Li, Shunian Chen, Peiyi Wang, Liang Chen, Yazheng Yang, Benyou Wang, and Lingpeng Kong. Silk: Preference distillation for large visual language models. *arXiv preprint arXiv:2312.10665*, 2023. 2
- [21] Xiang Lisa Li, Ari Holtzman, Daniel Fried, Percy Liang, Jason Eisner, Tatsunori Hashimoto, Luke Zettlemoyer, and Mike Lewis. Contrastive decoding: Open-ended text generation as optimization. *arXiv preprint arXiv:2210.15097*, 2022. 1
- [22] Yifan Li, Yifan Du, Kun Zhou, Jinpeng Wang, Wayne Xin Zhao, and Ji-Rong Wen. Evaluating object hallucination in large vision-language models. *arXiv preprint arXiv:2305.10355*, 2023. 6
- [23] Fuxiao Liu, Kevin Lin, Linjie Li, Jianfeng Wang, Yaser Yacoob, and Lijuan Wang. Mitigating hallucination in large multi-modal models via robust instruction tuning. In *The Twelfth International Conference on Learning Representations*, 2023. 2
- [24] Haotian Liu, Chunyuan Li, Yuheng Li, and Yong Jae Lee. Improved baselines with visual instruction tuning. In *Proceedings of the IEEE/CVF Conference on Computer Vision and Pattern Recognition*, pages 26296–26306, 2024. 1, 2, 6
- [25] Haotian Liu, Chunyuan Li, Qingyang Wu, and Yong Jae Lee. Visual instruction tuning. *Advances in neural information processing systems*, 36, 2024. 1, 2
- [26] Shi Liu, Kecheng Zheng, and Wei Chen. Paying more attention to image: A training-free method for alleviating hallucination in lvlms. *arXiv preprint arXiv:2407.21771*, 2024. 3, 12
- [27] Sean O’Brien and Mike Lewis. Contrastive decoding improves reasoning in large language models. *arXiv preprint arXiv:2309.09117*, 2023. 1
- [28] Anna Rohrbach, Lisa Anne Hendricks, Kaylee Burns, Trevor Darrell, and Kate Saenko. Object hallucination in image captioning. *arXiv preprint arXiv:1809.02156*, 2018. 6
- [29] Zhiqing Sun, Sheng Shen, Shengcao Cao, Haotian Liu, Chunyuan Li, Yikang Shen, Chuang Gan, Liang-Yan Gui, Yu-Xiong Wang, Yiming Yang, et al. Aligning large multi-modal models with factually augmented rlhf. *arXiv preprint arXiv:2309.14525*, 2023. 2
- [30] Hugo Touvron, Thibaut Lavril, Gautier Izacard, Xavier Martinet, Marie-Anne Lachaux, Timothée Lacroix, Baptiste Rozière, Naman Goyal, Eric Hambro, Faisal Azhar, et al. Llama: Open and efficient foundation language models. *arXiv preprint arXiv:2302.13971*, 2023. 1
- [31] Hugo Touvron, Louis Martin, Kevin Stone, Peter Albert, Amjad Almahairi, Yasmine Babaei, Nikolay Bashlykov, Soumya Batra, Prajwal Bhargava, Shruti Bhosale, et al. Llama 2: Open foundation and fine-tuned chat models. *arXiv preprint arXiv:2307.09288*, 2023. 1
- [32] Xintong Wang, Jingheng Pan, Liang Ding, and Chris Bie-mann. Mitigating hallucinations in large vision-language models with instruction contrastive decoding. *arXiv preprint arXiv:2403.18715*, 2024. 2, 3, 6, 12
- [33] Sangmin Woo, Jaehyuk Jang, Donguk Kim, Yubin Choi, and Changick Kim. Ritual: Random image transformations as a universal anti-hallucination lever in lvlms. *arXiv preprint arXiv:2405.17821*, 2024. 3, 12
- [34] Sangmin Woo, Donguk Kim, Jaehyuk Jang, Yubin Choi, and Changick Kim. Don’t miss the forest for the trees: Attentional vision calibration for large vision language models. *arXiv preprint arXiv:2405.17820*, 2024. 2, 3
- [35] Junfei Wu, Qiang Liu, Ding Wang, Jinghao Zhang, Shu Wu, Liang Wang, and Tieniu Tan. Logical closed loop: Uncovering object hallucinations in large vision-language models. *arXiv preprint arXiv:2402.11622*, 2024. 3
- [36] Qinghao Ye, Haiyang Xu, Guohai Xu, Jiabo Ye, Ming Yan, Yiyang Zhou, Junyang Wang, Anwen Hu, Pengcheng Shi, Yaya Shi, et al. mplug-owl: Modularization empowers large language models with multimodality. *arXiv preprint arXiv:2304.14178*, 2023. 2
- [37] Qinghao Ye, Haiyang Xu, Jiabo Ye, Ming Yan, Anwen Hu, Haowei Liu, Qi Qian, Ji Zhang, and Fei Huang. mplug-owl2: Revolutionizing multi-modal large language model with modality collaboration. In *Proceedings of the IEEE/CVF Conference on Computer Vision and Pattern Recognition*, pages 13040–13051, 2024. 2
- [38] Shukang Yin, Chaoyou Fu, Sirui Zhao, Tong Xu, Hao Wang, Dianbo Sui, Yunhang Shen, Ke Li, Xing Sun, and Enhong Chen. Woodpecker: Hallucination correction for multimodal large language models. *arXiv preprint arXiv:2310.16045*, 2023. 3
- [39] Qifan Yu, Juncheng Li, Longhui Wei, Liang Pang, Wentao Ye, Bosheng Qin, Siliang Tang, Qi Tian, and Yueting Zhuang. Hallucidoctor: Mitigating hallucinatory toxicity in visual instruction data. In *Proceedings of the IEEE/CVF Conference on Computer Vision and Pattern Recognition*, pages 12944–12953, 2024. 2
- [40] Tianyu Yu, Yuan Yao, Haoye Zhang, Taiwan He, Yifeng Han, Ganqu Cui, Jinyi Hu, Zhiyuan Liu, Hai-Tao Zheng, Maosong Sun, et al. Rllhf-v: Towards trustworthy mllms via behavior alignment from fine-grained correctional human feedback. In *Proceedings of the IEEE/CVF Conference on Computer Vision and Pattern Recognition*, pages 13807–13816, 2024. 2

- [41] Tianyu Yu, Haoye Zhang, Yuan Yao, Yunkai Dang, Da Chen, Xiaoman Lu, Ganqu Cui, Taiwen He, Zhiyuan Liu, Tat-Seng Chua, et al. Rlaif-v: Aligning mllms through open-source ai feedback for super gpt-4v trustworthiness. *arXiv preprint arXiv:2405.17220*, 2024. [2](#)
- [42] Zihao Yue, Liang Zhang, and Qin Jin. Less is more: Mitigating multimodal hallucination from an eos decision perspective. *arXiv preprint arXiv:2402.14545*, 2024. [2](#)
- [43] Bohan Zhai, Shijia Yang, Xiangchen Zhao, Chenfeng Xu, Sheng Shen, Dongdi Zhao, Kurt Keutzer, Manling Li, Tan Yan, and Xiangjun Fan. Halle-switch: Rethinking and controlling object existence hallucinations in large vision language models for detailed caption. *arXiv preprint arXiv:2310.01779*, 2023. [2](#)
- [44] Yiyang Zhou, Chenhang Cui, Jaehong Yoon, Linjun Zhang, Zhun Deng, Chelsea Finn, Mohit Bansal, and Huaxiu Yao. Analyzing and mitigating object hallucination in large vision-language models. *arXiv preprint arXiv:2310.00754*, 2023. [3](#)
- [45] Deyao Zhu, Jun Chen, Xiaoqian Shen, Xiang Li, and Mohamed Elhoseiny. Minigpt-4: Enhancing vision-language understanding with advanced large language models. *arXiv preprint arXiv:2304.10592*, 2023. [2](#)

## A. GPT-4o Assisted Evaluation

To assess the effectiveness of our method in mitigating hallucination beyond object existence during long-sequence generation, we conducted open evaluations of LVLG-generated responses using GPT-4o, as presented in Table 6. Following PAI [26], we sampled 50 images from the COCO dataset for image captioning tasks. Unlike PAI, which employs GPT4-V, we utilized the recently released GPT-4o to evaluate generated responses in terms of accuracy and detailedness. The GPT-4o prompts were designed in alignment with the structure in PAI [26]. We compare our method with the baseline method and existing decoding methods, including VCD[18] and ICD[32].

Our proposed method achieved superior GPT-4o scores compared to baseline and existing decoding approaches, reflecting its robustness under a more comprehensive evaluation framework. These results highlight the enhanced capability of our approach to generate more accurate and detailed responses for image captioning tasks.

Method	Accuracy $\uparrow$	Detailedness $\uparrow$
Baseline	5.38	5.88
Ours	6.65	6.45
VCD	5.83	5.93
Ours	6.57	6.54
ICD	6.03	6.48
Ours	6.61	6.52

Table 6. The results of LLaVA 1.5 for GPT-4o assisted evaluation. All the metrics are on a scale of 1 to 10.

## B. Detailed Comparison on CHAIR.

The *max new token* parameter plays a critical role in the evaluation on the CHAIR metric by restricting the maximum length of generated responses. In the main text, we present results under the settings *max new token* = 1024 and *top p* = 1. Additionally, following [13, 33], we also report results for *max new token* = 64 in Table 7.

As illustrated in the table, the *max new token* value significantly influences the performance of LVLGs on the CHAIR metric. Nevertheless, our method outperforms other methods by a clear margin. It shows our method consistently demonstrates superior hallucination mitigation capabilities, further validating its robustness and effectiveness under a strict constraint on the length of generated responses.

## C. Inference Time Analysis

To validate the effectiveness of our method on the inference speed, we estimate the inference time consumption

Method	CHAIR <sub>i</sub> $\downarrow$	CHAIR <sub>s</sub> $\downarrow$	Recall $\uparrow$	F1 Score $\uparrow$
Baseline	25.4	9.1	56.7	69.8
VCD	22.0	6.9	62.0	74.4
ICD	22.2	7.8	61.1	73.5
Ours	20.5	6.1	62.6	75.1

Table 7. Results of CHAIR on the MS-COCO validation set with the *max new token* = 64.

of MLLMs employing different decoding strategies in the POPE dataset in table 8. The results demonstrate that our proposed method achieves faster inference speeds compared to existing methods such as VCD and ICD. This improvement stems from IMCCD’s ability to directly derive the attention weights and key-value vectors for the distorted forward process from the original forward process, avoiding redundant computations. However, it is also observed that the inclusion of CDAR slightly reduces inference speed due to the additional computation of attention logits refined with position embeddings.

Method	Inference speed(tokens/s)
Baseline	12.93
VCD	7.04
ICD	6.90
Ours(CMVED only)	7.75
Ours(CMVED+CDAR)	7.38

Table 8. Ablation of different kinds of distortion used in our method.

## D. More Analysis of CDAR

To further validate the effectiveness of CDAR, We analyze the attention distribution from text tokens to image tokens with and without position embeddings by visualizing the attention maps. Specifically, we estimate the average attention from the final text token to each image token using data from the POPE dataset. As depicted in Figure 6(a), when position embeddings are included, the text tokens predominantly focus on the latter portion of the visual content, neglecting other relevant regions. Conversely, as in Figure 6(b), removing the position embeddings significantly enhances attention to all image tokens. It shows that the position embeddings lead to position bias in the attention mechanism. CDAR eliminates the position relation among different image tokens on the cross-modal part in the initial layers to mitigate the overlooking of critical visual information.

We also conduct more ablation about the variants of position embedding strategy in CDAR in Table 9. Noth that "with position embedding" demotes estimating the attention

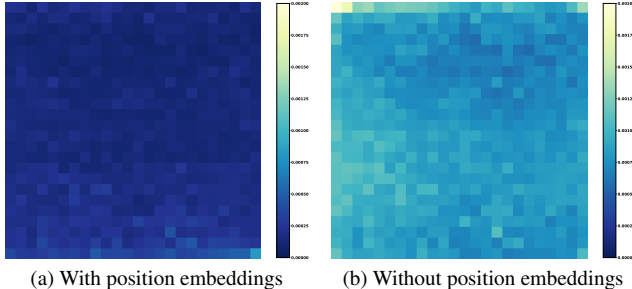


Figure 6. The attention distribution of text tokens to image tokens with (a) and without (b) the position embeddings.

logits with position embeddings, which is equal to directly removing the CDAR in our method. When removing the position embeddings to estimate the refined attention logits, the performance of MLLMs improves compared to the conventional design with position embeddings. It demonstrates that the position relations of image tokens result in an overlook of the former but relevant visual content. Additionally, the refined position embeddings used in CDAR further lead to an improvement, which shows the significance of the global positional relation of the image content with other language tokens.

Distortion	POPE		CHAIR	
	Accuracy	F1 Score	CHAIR <sub>i</sub>	CHAIR <sub>s</sub>
with position embeddings	85.86	85.51	50.6	14.3
remove position embeddings	86.21	86.12	50.0	13.9
refined position embeddings	86.73	86.13	49.8	13.8

Table 9. Ablation of different variants of position embedding strategy used in our method.

## E. Qualitative results of long sequence response

To further validate the effectiveness of our method, we present some cases of long sequence response in image captioning tasks in Figure 7 and Figure 8. These examples illustrate the proposed IMCCD approach effectively mitigates hallucinations in the generated responses, providing more accurate and contextually relevant descriptions compared to baseline methods.

## F. Choices of Hyper-parameters

In this section, we analyze the choices of hyper-parameters used in the proposed approach, including  $\alpha$ ,  $l$ , and  $\gamma$ .

**Choice of  $\alpha$ .**  $\alpha$  is the most important parameter for the contrastive decoding, which moderates the contrastive effect. To determine the value of  $\alpha$ , we compared model performance under different  $\alpha$  for existing decoding method

VCD and our method in Table 10. Compared with the performance under  $\alpha = 1$ , our method shows a better performance under a more aggressive setting  $\alpha = 3$  while VCD demonstrates improvement on the MS-COCO dataset but suffers a performance decline on GQA under  $\alpha = 3$ . These results indicate that our method more accurately estimates a distorted distribution favoring hallucination mitigation, demonstrating greater robustness across different  $\alpha$  values.

$\alpha$	Method	COCO		GQA	
		Accuracy $\uparrow$	F1 Score $\uparrow$	Accuracy $\uparrow$	F1 Score $\uparrow$
1	VCD	85.38	85.06	80.73	82.24
	Ours	85.97	85.63	83.55	83.24
3	VCD	85.70	85.51	80.47	82.28
	Ours	86.47	86.17	84.00	84.81
5	VCD	85.73	85.58	80.33	82.21
	Ours	86.83	87.61	84.13	84.97

Table 10. The performance of VCD and our method under the different values of  $\alpha$  on LLaVA 1.5.

**Choice of  $l$ .** Table 11 presents the performance of our IMCCD approach on LLaVA 1.5 under varying values of  $l$ . Increasing  $l$  from 1 to 3 improves performance on both the POPE and CHAIR benchmarks, demonstrating that a higher  $l$  effectively reduces the hallucination from the overlook of relevant visual content. However, performance on the CHAIR benchmark declines when  $l$  is set to 5 compared to  $l = 3$ . This reduction likely occurs because the latter tokens for visual content often summarize preceding visual information, which is particularly beneficial for image captioning tasks. These results suggest that choosing a smaller  $l$  helps preserve the contribution of summary tokens in later layers, enhancing performance in tasks like image captioning.

$l$	POPE		CHAIR	
	Accuracy $\uparrow$	F1 Score $\uparrow$	CHAIR <sub>i</sub> $\downarrow$	CHAIR <sub>s</sub> $\downarrow$
1	86.21	85.94	50.0	13.9
3	86.47	86.17	49.8	13.8
5	86.62	86.36	50.5	14.4

Table 11. The performance of our method under the different values of  $l$  on LLaVA 1.5.

**Choice of  $\gamma$ .** To better select  $\gamma$ , we present its performance under different settings in Table 12. The results indicate that our method is not overly sensitive to the choice of  $\gamma$ . Setting  $\gamma$  to 0.1 or 0.3, as opposed to the default 0.2, only leads to a slight decrease in the LVLM performance.



Please describe this image in detail.



The image captures a large, majestic elephant walking through a field with a lush green forest surrounding it. The elephant strolls casually along an area of dirt and **is accompanied by a small or juvenile elephant close by, a little smaller than the main one.** The elephants are walking through a flowing river, their trunks up near them, possibly as an indication of their presence or curiosity about the water. The scene constitutes a serene and picturesque snapshot of an elephant-filled forest in its natural habitat.



Normal

The image features an elephant walking across a lush green field, surrounded by a forest. The elephant is positioned towards the right side of the scene, making its way across the landscape. In the background, there is **a bird perched on a tree branch,** adding a touch of wildlife diversity to the scene. The field is filled with grass and appears to be a part of the elephant's natural habitat.



VCD

The image features a large elephant standing alone in a grassy field, close to a watering hole. The elephant is facing the camera and appears to be enjoying the natural surroundings. The scene is lush and green, with trees surrounding the area and a body of water nearby. The elephant's presence in this serene environment highlights the beauty of nature and the majesty of these majestic animals.



Ours



Please describe this image in detail.



A young girl and a boy are standing in their living room playing a video game on a Wii gaming console. The girl appears to be holding a Wii remote, while both children enjoy the game being displayed on the television. The TV is centered towards the background of the scene, and a couch can be spotted behind them, slightly to the right. The room also has multiple books scattered around, likely for the family to read leisurely, showcasing the comfortable and entertaining atmosphere in the living space.



Normal

The image features a living room with a television situated in the middle of the scene. Two children, a boy and a girl, are playing a video game on the Wii console, each holding a remote in their hands. They are standing close to the television, fully engaged in the game. The room also contains several books scattered around, some of which are placed on a bookshelf and others are lying on the floor. **A clock is mounted on the wall, and there is a handbag placed near the right edge of the image. Additionally, there is a bowl and a cup placed in the room, possibly for refreshments during their gaming session.**



VCD

The image depicts a young girl and a boy playing a baseball video game together on a flat screen TV in a living room. The girl is standing on the right side of the scene, while the boy is positioned on the left side. They both hold remotes in their hands, actively engaged in the game. The living room features a TV mounted on the wall, a bookcase filled with various books, and a small basket on a surface near the TV.



Ours

Figure 7. Qualitative results of different methods on MS-COCO image captioning task. The hallucinated content is highlighted in red.



Please describe this image in detail.



In the image, a large bird is perched on top of a parking meter on the side of a busy street. The street is filled with traffic, as various cars, trucks, a bus, and a motorcycle occupy the scene. Some vehicles are parked along the street, while others are in motion. The setting seems to be urban, with traffic lights present in many different parts of the scene. Some city benches are visible, likely sitting near the curb for people to rest or wait. The bird dominates the foreground, standing out from the bustling street environment.



Normal

The image features a crowded street scene with a black bird perched on a parking meter, possibly waiting for its turn to cross the road. The street is filled with various vehicles, including several cars, a bus, and a truck. In addition to the cars, there are two traffic lights visible in the scene, one located towards the left side and another closer to the right. A person can be seen standing near the center of the scene, possibly waiting to cross the street or simply observing the bustling environment.



VCD

The image features a black bird perched on a parking meter next to a car. The bird appears to be looking inside the car window, possibly searching for food. The car is parked on the side of the street, and there are several other vehicles in the scene. In addition to the car with the bird, there are four other cars parked or driving nearby. There are also two traffic lights visible, one at the top left corner and another closer to the center of the scene. A truck can be seen on the left side of the image, possibly indicating ongoing construction or maintenance work in the area.



Ours



Please describe this image in detail.



The scene features a woman standing in the grass in front of a building, throwing something possibly a frisbee or kite for her cat to chase or play with. A cat in the area seems to be watching the kite or toy in motion. Another person can be seen nearby, standing at a distance from the cat. A fire hydrant is visible in the background, located near the right side of the image, and the playground can be seen in the far right corner. The overall setting is an outdoor environment with grassy areas and buildings.



Normal

The image features a young boy flying a kite in a backyard, with a cat watching nearby. The boy is holding onto the kite string, which is visible in the scene. The cat is lying in the grass, observing the kite's movements. In the background, there are two parked cars, one on the left side and the other on the right side of the scene. Additionally, there is a bottle located near the center of the image, possibly belonging to the boy or someone else in the yard.



VCD

In the image, a person is flying a kite in a green yard near a white house. The kite can be seen soaring in the sky, while the person stands on the grass holding the kite string. There is also a cat lying on the grass, watching the kite as it flies overhead. The yard is well-maintained with a sidewalk visible, and a street can be seen nearby. The scene conveys a leisurely and relaxed atmosphere, as the person enjoys the outdoors with their cat.



Ours

Figure 8. Qualitative results of different methods on MS-COCO image captioning task. The hallucinated content is highlighted in red.

$\gamma$	POPE		CHAIR	
	Accuracy $\uparrow$	F1 Score $\uparrow$	CHAIR $_i$ $\downarrow$	CHAIR $_s$ $\downarrow$
0.1	85.98	85.86	50.0	13.9
0.2	86.73	86.13	49.8	13.8
0.3	86.32	86.11	50.6	14.4

Table 12. The performance of our method under the different values of  $\gamma$  on LLaVA 1.5.

## G. Limitations

Our method notably enhances the inference performance of LVLMs by effectively addressing hallucination issues. In the CMVED module, we mitigate spurious inter-modality correlations by selectively masking value vectors based on the magnitude of attention weights. However, the magnitude of attention weights may not fully capture the causal relevance between text and visual tokens. Developing a more refined selection mechanism could enable a more accurate estimation of distorted distributions, further improving performance.

Additionally, since IMCCD does not enhance the visual encoder’s ability to extract and represent relevant knowledge from images, its effectiveness remains constrained by the grounding capability of the visual encoder. Future work will explore these directions to achieve more robust and comprehensive improvements.